Optics Communications 312 (2014) 31–34

Contents lists available at ScienceDirect

Optics Communications

journal homepage: www.elsevier.com/locate/optcom

Polarization-dependent photocurrent enhancement in metamaterial-coupled quantum dots-in-a-well infrared detectors

Yagya D. Sharma [a], Young Chul Jun [b,c,d,*], Jun Oh Kim [a], Igal Brener [b,c], Sanjay Krishna [a]

[a] Center for High Technology Materials, University of New Mexico, NM 87106, USA
[b] Sandia National Laboratories, NM 87185, USA
[c] Center for Integrated Nanotechnologies, Sandia National Laboratories, NM 87185, USA
[d] Department of Physics, Inha University, Incheon 402-751, Republic of Korea

ARTICLE INFO

Article history:
Received 26 June 2013
Received in revised form
13 July 2013
Accepted 3 September 2013
Available online 19 September 2013

Keywords:
Metamaterial
Plasmonic field enhancement
Infrared photodetectors

ABSTRACT

We demonstrate polarization-dependent photo-response enhancement in metamaterial-coupled quantum dots-in-a-well infrared detectors. A gold split-ring resonator metamaterial layer was patterned by electron-beam lithography in the detector aperture. In this integrated structure, the detector spectral response is given by the convolution of the metamaterial field enhancement and the original detector response. Our polarization-resolved measurement unambiguously shows that the spectral response can be strongly modified by metamaterial patterning. When the metamaterial resonance matches the QD absorption peak, we obtain a clear enhancement of generated photocurrent. Various metamaterial designs can be employed to implement multi-functional detector structures.

1. Introduction

Infrared (IR) photodetectors have various applications, ranging from thermal imaging to medical diagnostics. Over the last decade, new materials and structures have been introduced to improve detector performances, such as spectral sensitivity, peak wavelength tunability, leakage current level, and operating temperature. Among them, quantum dots-in-a-well (DWELL) infrared detectors have attracted attention recently [1–3]. It combines superior peak wavelength control of quantum well IR detectors with the reduced dark current and normal incidence operation of quantum dot (QD) IR detectors. At the same time, there has been increasing interest in using plasmonic field enhancement for photodetectors [4–7]. Resonantly excited plasmonic resonators can provide strong near-fields to enhance light absorption and improve the detector performance.

In this paper, we integrate a plasmonic metamaterial (MM) structure with DWELL IR detectors, and demonstrate that MM patterning can be an effective method for controlling IR detector response. In fact, there have been several studies to use plasmonic structures for IR detectors [8–11]. But those patterns were limited to simple metal hole array or grating structures of micro-meter feature sizes. In our work, we use deep subwavelength, nano-meter scale split-ring resonator (SRR) structures patterned by electron-beam lithography. Our polarization-resolved photocurrent measurements clearly demonstrate that the detector spectral response can be tailored by pattering on the detector aperture surface. Especially, when the MM resonance matches the QD absorption peak frequency, we obtain a strong photocurrent enhancement of about 100%. The use of electron-beam lithography makes our work extendable to many other complicated MM patterns. For instance, MM resonances can be designed to be extremely narrow-banded [12–14] or sensitive to vortex beams [15]. These engineered surface patterns can eventually enable highly functional, monolithically integrated IR detectors.

2. Sample fabrication

The QD detectors were grown by molecular beam epitaxy (MBE) with an As_2 cracker source. It was grown on an n+ doped GaAs substrate to avoid substrate scattering and optical cross talk. In our DWELL design, InAs QDs were placed in an asymmetric InGaAs quantum well (Fig. 1a). This was again separated by an $Al_{0.07}Ga_{0.93}As$ barrier. The active layer consists of 7 periods of DWELL stacks. The QD absorption in the current detector structure occurs in the mid-IR range of 5–8 μm.

Arrays of 410 μm by 410 μm detector mesas with a top pixel aperture of 300 μm in diameter were defined using optical lithography (Fig. 1a), followed by inductively coupled plasma etching and electron-beam evaporation of metal contacts. Both top and bottom contacts were annealed at 380 °C using rapid thermal annealing to obtain ohmic contacts. Before patterning MM structures, we

* Corresponding author at: Department of Physics, Inha University, Incheon 402-751, Republic of Korea. Tel.: +82 32 860 8845.
E-mail address: youngchul.jun@inha.ac.kr (Y.C. Jun).

0030-4018
http://dx.doi.org/10.1016/j.optcom.2013.09.010

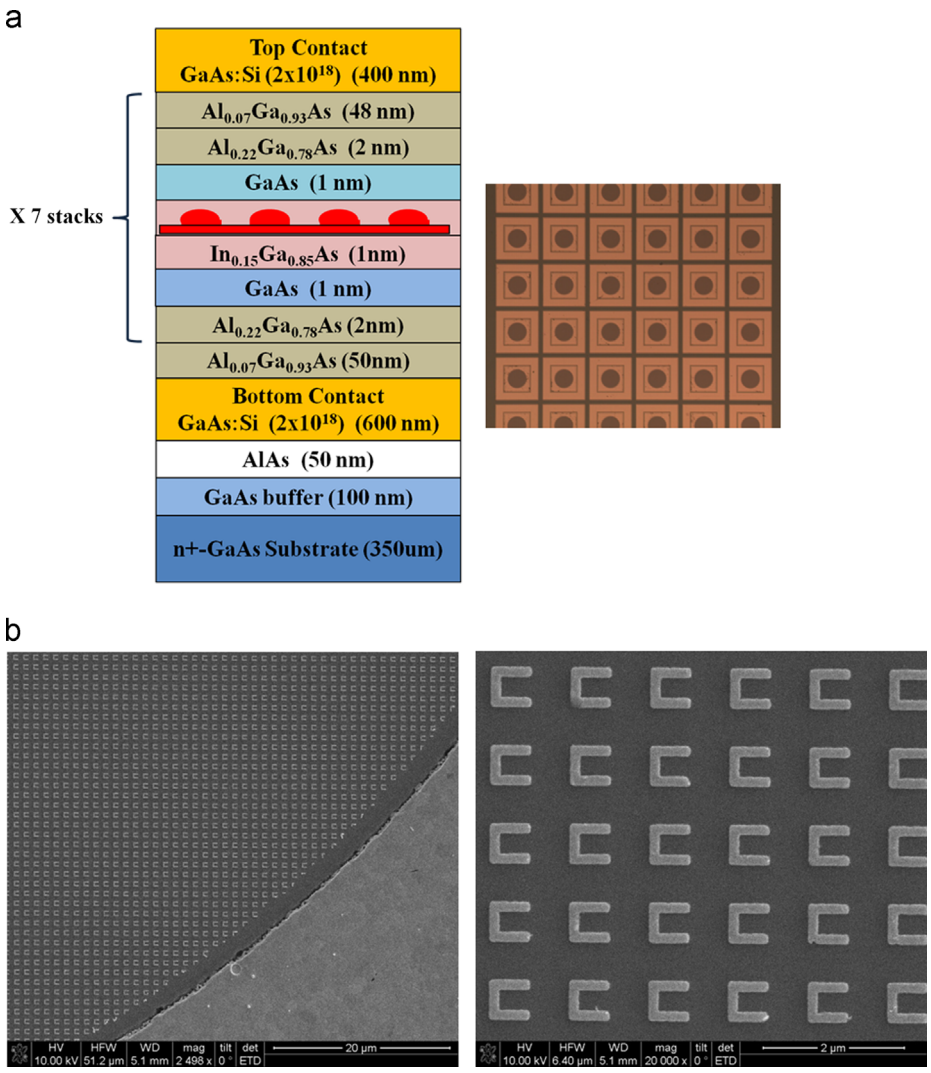

Fig. 1. (a) Schematic of the DWELL structure and the optical microscope image of detector mesa arrays. Each detector has top and bottom contacts, and the top contact has an aperture of 300 μm in diameter for light detection. (b) The scanning electron microscope image of the gold SRR array. SRR arrays with different scale factors (i.e. different geometric sizes) are patterned in the detector apertures by electron-beam lithography.

etched down the top n+ contact layer in the pixel aperture by ~390 nm to bring the MM layer closer to the QD region. We left a very thin (~10 nm) n+ GaAs top contact layer to ease carrier collection.

The MM structure in the pixel aperture area was patterned by electron-beam lithography, metal evaporation, and liftoff (Fig. 1b). Due to the height of pixel mesas (~850 nm), we first planarized the detector array by spin-coating photoresist and baking. After making an opening on the aperture surface with optical lithography, we spin-coated PMMA (i.e. ebeam resist) on top and went through the normal ebeam lithography sequence. We fabricated arrays of SRRs with different scale factors to gradually tune the MM resonance frequencies.

3. Numerical simulation and analysis

The resonance behavior of our MM layer was first studied by numerical simulation. We used typical c-shaped SRRs as our MM layer. We performed finite difference time domain (FDTD) simulations which include our QD IR detector substrate (Fig. 1a) and a unit cell of SRR (Fig. 1b). A broadband light pulse was incident from the top and the transmission was measured on the substrate side to characterize SRR resonances. SRR resonance wavelengths could be gradually tuned by geometric scaling (i.e. SRR scale factor). The polarization of incident light was either normal (Fig. 2a) or parallel (Fig. 2b) to the SRR gap. Fig. 2 shows the simulated transmission spectra for two polarizations. The transmission has a dip at the SRR resonance frequency. For normal polarization, the SRR exhibits a LC-type resonance, and its resonance frequency spans the QD absorption range (5–8 μm) for the SRR scale factors of 0.6–0.8. However, for parallel polarization, the SRR structure does not show resonant behavior in the same wavelength range (5–8 μm).

Field enhancement from the MM layer follows this resonant behavior. Fig. 3 shows the simulated electric field distribution. The strong field enhancement on the substrate for normal polarization (Fig. 3a,b) is in stark contrast to a much weaker field distribution for parallel polarization (Fig. 3c,d).

It is also noteworthy that parallel polarization excites a different type of resonances at very short wavelengths (≤ 4 μm). From the simulated field distribution on the SRR, we find that this is a dipole-type resonance existing on the two arms of SRR. The directions of electron oscillations are indicated as dotted arrows for two polarizations in Fig. 2a and b.

4. Photocurrent measurement

The fabricated sample was mounted in a cryostat and cooled down to liquid nitrogen temperature at 77 K. The spectral response was measured using a Nicolet 6700 Fourier transform infrared spectrometer (FTIR) at a bias of −3.5 V. Fig. 4a shows the photocurrent spectra from a reference sample (which does not have MM patterning). This just shows a spectral response of the original QD IR detector. QD absorption occurs in the range of 5–8 μm and has two prominent peaks at 5.5 μm and 7 μm. Because we do not have any surface patterning, the spectral response for two polarizations should be the same. But, we actually have a slight difference between them: the parallel polarization (i.e. 90°) has slightly larger spectral response than the normal polarization (i.e. 0°) at 7 μm. We attribute this to the anisotropic shape of the QDs.

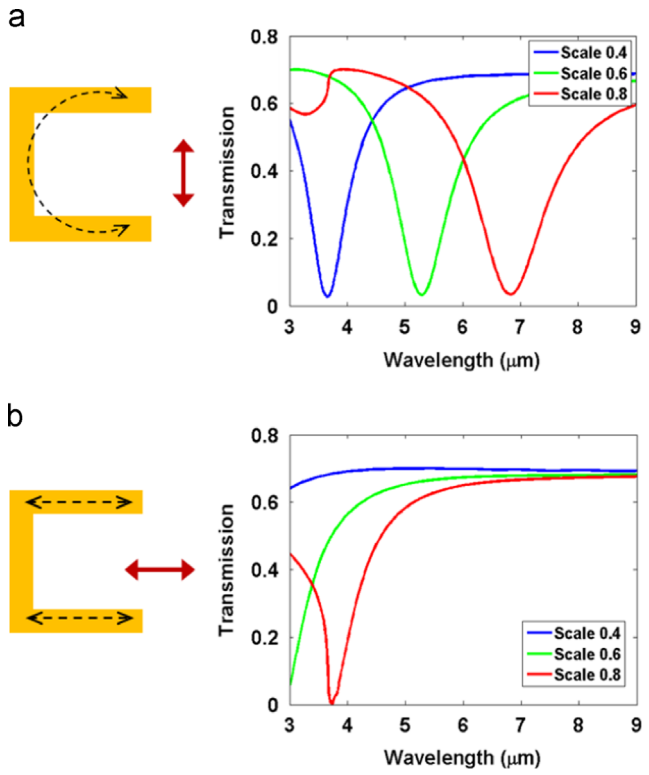

Fig. 2. Simulated transmission spectra through the metamaterial-detector structure for (a) normal polarization and (b) parallel polarization of incident light. Dotted black lines on the SRR schematic show the directions of electron oscillations for the two incident polarizations. The arm length and thickness of the gold SRR are 680 nm and 140 nm for a scale factor 1.

We patterned SRR structures with different scale factors (i.e. with different geometric sizes) to gradually tune MM resonance frequencies. Fig. 4b–d shows the spectral response for scale factors 0.7, 0.8, and 0.9. When the incident light is polarized normal to the gap (i.e. 0°) and the SRR resonance matches the QD absorption peak at 7 μm (scale factor 0.8), the obtained photocurrent exhibits clear photocurrent enhancement about a factor of two (red curve in Fig. 4c). But, the other polarization (90°, black line in Fig. 4c) does not produce a noticeable change, compared to that from the reference sample. We also see different spectral responses for two other scale factors. With a smaller scale factor 0.7 (i.e. the SRR resonance shifts to a shorter wavelength), we have photocurrent enhancement between 6 and 7 μm (red curve in Fig. 4b), while with a larger scale factor 0.9 (i.e. the SRR resonance shifts to a longer wavelength), we have more enhancement in the region longer than 7 μm (red curve in Fig. 4d).

The experimental results agree with our numerical simulations. As the scale factor increases from 0.7 to 0.9, the SRR resonance shifts from ~6 μm to ~7.5 μm. Field enhancement from SRRs also follows this resonance behavior. The spectral response is the convolution of this field enhancement and the original detector response (Fig. 4a). Therefore, we obtain the spectral behaviors as shown in Fig. 4b–d.

The other polarization (90°) does not excite the SRR resonance. Therefore, the spectral responses for parallel polarization (black curves in Fig. 4b–d) are almost the same as that from the reference sample. However, we find one interesting feature for the scale factor 0.9 at a very short wavelength (~4 μm) (see the green dotted line in Fig. 4d). We have an additional photocurrent peak for the parallel polarization. As we have seen in Fig. 2b, a parallel

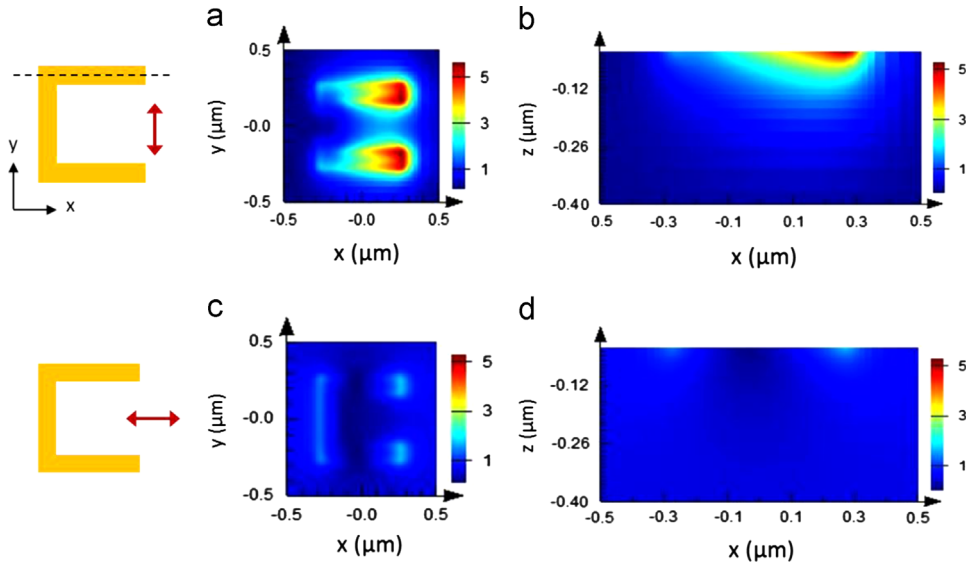

Fig. 3. Electric field distribution for two polarizations: (a) and (b) are for the normal polarization of incident light, while (c) and (d) are for the parallel polarization. The electric field magnitude is normalized to the free-space value ($|E|/|E_0|$). The field magnitude profile in the *xy* plane (a,c) is measured 30 nm below the SRR–semiconductor interface. The field magnitude profile in the *xz* plane (b,d) is measured along the SRR arm (dotted line in the upper, left SRR schematic) onto the substrate. The field distribution was obtained for the SRR with a scale factor 0.8 at $\lambda_0 = 6.9$ μm. Two polarizations exhibit a clear difference in field enhancement on the substrate and this, in turn, affects photocurrent enhancement in the detector.

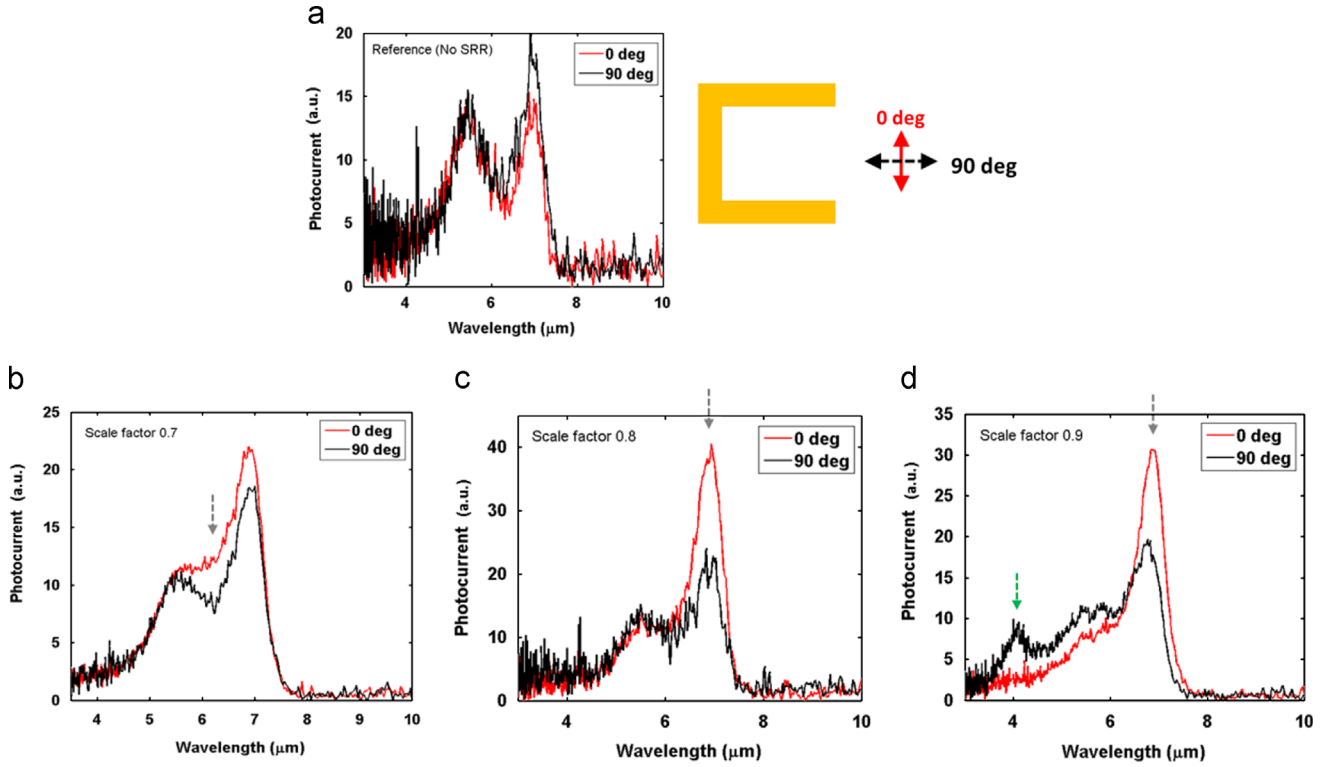

Fig. 4. Photocurrent spectra for two incident polarizations, measured from (a) a reference sample (i.e. no SRR patterns) and (b)–(d) metamaterial-patterned detector samples. In (b)–(d), the SRR scale factors are 0.7, 0.8, and 0.9. (For interpretation of the references to color in this figure, the reader is referred to the web version of this article.)

polarization beam can excite dipole-type resonances at very short wavelengths (4 μm or below). Again, this spectral feature agrees with our numerical simulation.

In this work, we used a simple c-shaped SRR structure to investigate the MM-coupled IR detector response. However, various deep subwavelength MM structures can be fabricated by electron-beam lithography. For example, MM resonances can be made to be more polarization specific (e.g. sensitive to circular polarization). MM resonances can be designed to be either narrow-banded or broad-banded, depending on the detector purpose. Or they can be excited for a specific angle of incidence only. Many new IR detector functionalities can be implemented simply by designing suitable MM structures.

5. Conclusions

In conclusion, we have studied MM-coupled IR detector responses. Our polarization-resolved photocurrent measurements clearly show that the detector spectral response is affected by MM pattering on the detector aperture surface. When the MM resonance matches the QD absorption peak, we obtain a prominent enhancement of photocurrent. These observations are supported by numerical simulations too. Various detector functionalities can be implemented by proper MM patterning on the detector surface. This can lead to highly compact, fully integrated IR detector systems.

Acknowledgments

This work was performed, in part, at the Center for Integrated Nanotechnologies, an Office of Science User Facility operated for the U.S. Department of Energy (DOE) Office of Science. Sandia National Laboratories is a multi-program laboratory managed and operated by Sandia Corporation, a wholly owned subsidiary of Lockheed Martin Corporation, for the U.S. Department of Energy's National Nuclear Security Administration under contract DE-AC04-94AL85000. Support from the KRISS-UNM Global Research Laboratory Program (No. 2007-00011) is acknowledged. YCJ acknowledges the support from the MSIP (Ministry of Science, ICT&Future Planning), Korea, under the ITRC (Information Technology Research Center) support program (NIPA-2013-H0301-13-1010) supervised by the NIPA (National IT Industry Promotion Agency).

References

[1] G.T. Liu, A. Stintz, H. Li, T.C. Newell, A.L. Gray, P.M. Varangis, K.J. Malloy, L.F. Lester, IEEE Journal of Quantum Electronics 36 (2000) 1272.
[2] S. Raghavan, P. Rotella, A. Stintz, B. Fuchs, S. Krishna, C. Morath, D.A. Cardimona, S.W. Kennerly, Applied Physics Letters 81 (2002) 1369.
[3] A.V. Barve, S.J. Lee, S.K. Noh, S. Krishna, Laser and Photonics Reviews 4 (2010) 738.
[4] J.A. Schuller, E.S. Barnard, W. Cai, Y.C. Jun, J.S. White, M.L. Brongersma, Nature Materials 9 (2010) 193.
[5] T. Ishi, T. Fujikata, K. Makita, T. Baba, K. Ohashi, Japanese Journal of Applied Physics 44 (2005) 364.
[6] L. Tang, S.E. Kocabas, S. Latif, A.K. Okyay, D.-S. Ly-Gagnon, K.C. Saraswat, D.A.B. Miller, Nature Photonics 2 (2008) 226.
[7] A. Farzaneh, J.S. White, W. Cai, M.L. Brongersma, Nanophotonics 1 (2012) 125.
[8] Z. Yu, G. Veronis, S. Fan, M.L. Brongersma, Applied Physics Letters 89 (2006) 151116.
[9] J. Rosenberg, R.V. Shenoi, T.E. Vandervelde, S. Krishna, O. Painter, Applied Physics Letters 95 (2006) 161101.
[10] C.-C. Chang, Y.D. Sharma, Y.-S. Kim, J.A. Bur, R.V. Shenoi, S. Krishna, D. Huang, S.-Y. Lin, Nano Letters 10 (2010) 1704.
[11] S.J. Lee, Z. Ku, A. Barve, J. Montoya, W.-Y. Jang, S.R.J. Brueck, M. Sundaram, A. Reisinger, S. Krishna, S.K. Noh, Nature Communications 2 (2011) 286.
[12] V.A. Fedotov, M. Rose, S.L. Prosvirnin, N. Papasimakis, N.I. Zheludev, Physical Review Letters 99 (2007) 147401.
[13] R. Adato, A.A. Yanik, J.J. Amsden, D.L. Kaplan, F.G. Omenetto, M.K. Hong, S. Erramilli, H. Altug, Proceedings of the National Academy of Sciences United States of America 106 (2009) 19227.
[14] V.V. Khardikov, E.O. Iarko, S.L. Prosvirnin, Journal of Optics 12 (2010) 045102.
[15] P. Genevet, J. Lin, M.A. Kats, F. Capasso, Nature Communications 3 (2012) 1278.